PROCEEDINGS OF SCIENCE

Half-lives of neutron-rich nuclei around ^{35,36}Mg

K. Steiger[*,1] **S. Nishimura**,[2] **Z. Li**,[2,3] **R. Chen**,[2] **T. Faestermann**,[1] **R. Gernhäuser**,[1] **C. Hinke**,[1] **R. Krücken**,[1,4] **M. Kurata-Nishimura**,[2] **G. Lorusso**,[2] **Y. Miyashita**,[5] **K. Sugimoto**,[5] **T. Sumikama**,[6] **H. Watanabe**,[7] **K. Yoshinaga**[5]

[1] *Physik-Department E12, Technische Universität München, 85748 Garching, Germany*
[2] *RIKEN Nishina Center, 2-1 Hirosawa, Wako, Saitama 351-0198, Japan*
[3] *Department of Physics, Peking University, Beijing 100871, China*
[4] *TRIUMF, 4004 Wesbrook Mall, Vancouver, BC V6T2A3, Canada*
[5] *Department of Physics, Tokyo University of Science, 2641 Yamazaki, Noda, Chiba 278-8510, Japan*
[6] *Department of Physics, Tohoku University, Aoba, Sendai, Miyagi 980-8578, Japan*
[7] *Department of Physics, Beihang University, Beijing 100191, China*
E-mail: konrad.steiger@ph.tum.de

We performed a decay spectroscopy experiment investigating neutron-rich nuclei around ^{35,36}Mg at the RIBF (Radioactive Isotope Beam Factory, RIKEN, Japan). These nuclei were produced by relativistic projectile fragmentation of a 345 AMeV ^{48}Ca primary beam from the superconducting ring cyclotron SRC with an average intensity of 70 pnA. The secondary cocktail beam was separated and identified with the BigRIPS [1] fragment separator and the ZeroDegree spectrometer (ZDS). The unambiguous particle identification was achieved by the multiple measurement of the energy loss (ΔE), time of flight (TOF) and magnetic rigidity ($B\rho$) event-by-event. The identified fragments were implanted in the CAITEN [2] detector (Cylindrical Active Implantation Target for Efficient Nuclear-decay study). The main part of this detector is a highly segmented plastic scintillator with the shape of a hollow cylinder. To reduce background decay events the scintillator was rotated and in additiom moved vertically. Implantations and decays were correlated in time and space to determine precise half-lives for the implanted nuclei.

International Winter Meeting on Nuclear Physics,
21-25 January 2013
Bormio, Italy

[*]Speaker.

PoS(Bormio 2013)032

1. Introduction

The half-life is the first observable which is accessible in pioneering experiments investigating very exotic nuclei. The experiment discussed in this work was performed in fall 2010 at the Radioactive Isotope Beam Factory (RIBF) [3] at the RIKEN Nishina Center for Accelerator-Based Science which is located at Wako (Saitama Prefecture), Japan. Decay properties of neutron-rich nuclei in the area around ^{35,36}Mg were investigated. These nuclei were produced by relativistic projectile fragmentation. They were separated and identified in flight using the BigRIPS spectrometer and stopped in an implantation detector to perform decay spectroscopy.

2. Experimental setup

2.1 Separation and identification

Neutron-rich nuclei were produced via relativistic projectile fragmentation of $^{48}Ca^{20+}$ projectiles from the Superconducting Ring Cyclotron (SRC) with an energy $E = 345A$ MeV, incident on a rotating beryllium target with a thickness of 15 mm which corresponds to an areal density of 2.8 g/cm^2. The nuclei of interest were separated and identified with the BigRIPS spectrometer [1]. The separation of background fragments in the cocktail beam was done with the first stage of the BigRIPS fragment separator. Two dipole magnets and an achromatic aluminum energy degrader located at the dispersive focus F1 were used to perform a $B\rho$-ΔE-$B\rho$ selection. The dipole magnets separate the beam with respect to the magnetic rigidity $B\rho$ and the transmission of the beam through a degrader results in an energy loss ΔE which depends on the nuclear charge Z of the transmitted fragment. To study different regions of interest on the nuclear chart, two different settings of the spectrometer with ^{30}Ne and ^{36}Mg as a central fragment had been used. The degrader had a median thickness of 15 mm and 10 mm for the ^{30}Ne and ^{36}Mg setting, respectively. The second stage of BigRIPS (F3 to F7) was used to identify the transmitted fragmentation products using the ΔE-$B\rho$-velocity method. The energy loss ΔE of the ions was measured in a multi-sampling ionization chamber (MUSIC) located at F7. The magnetic rigidity $B\rho$ was determined from position measurements of parallel plate avalanche counters (PPAC) [4] at the achromatic focus F3, the dispersive focus F5 and the achromatic focus F7. The time of flight (TOF) was measured between two plastic scintillators at F3 and F7 separated by a flight path of 47 m. With this information an unambiguous event-by-event identification of the fragments in (A,Z) is possible. A second identification of the beam fragments was performed in the zero-degree spectrometer (ZDS). The ΔE-$B\rho$-velocity method was applied again between the focal planes F8 to F11. The result of the particle identification of the ZDS can be seen in figure 1. At the end of the beam line (F11) the identified fragments were stopped in the implantation detector CAITEN described in the next section.

2.2 Implantation and beta detector CAITEN

CAITEN [2] (Cylindrical Active Implantation Target for Exotic Nuclei) is a highly segmented implantation and β detector. It can handle high implantation rates up to several kHz of heavy ion cocktail beams and is able to measure half-lives in the range of milliseconds up to several hundreds of milliseconds. It consists of two subsystems: A segmented movable hollow-cylindrical-shape plastic scintillator and 24 stationary position-sensitive photomultiplier tubes (PSPMTs) arranged

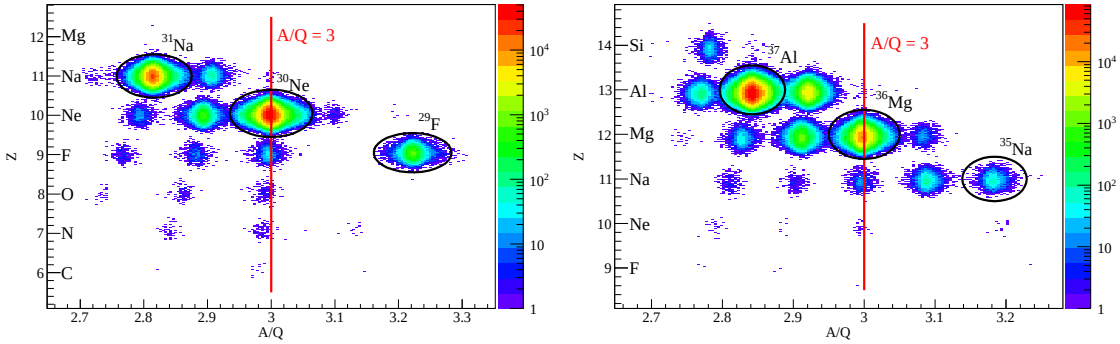

Figure 1: Particle identification in the ZDS between F8 and F11. The mass resolution of the ZDS is $\Delta A = 0.23$ (FWHM) and the nuclear charge resolution is $\Delta Z = 0.30$ (FWHM). *Left:* ^{30}Ne setting. $N = 20$ isotones are marked in black. *Right:* ^{36}Mg setting. $N = 24$ isotones are marked in black.

on a ring inside the scintillator at the height of the beam line. Implantations and decays are detected with position and time information. A schematic view of the CAITEN components is shown in the left part of figure 2. The implantation region of the detector is surrounded by 3 HPGe clover detectors not used in the analysis described in this paper.

2.2.1 Scintillator

The scintillator has a diameter of 500 mm, a height of 1000 mm and a thickness of 20 mm. It is highly segmented and is made of $4 \cdot 10^4$ plastic pixels of the size $6 \times 6 \times 20\,\text{mm}^3$. They are separated from each other by a thin mesh made from aluminum sheets. To reduce background events the scintillator is rotating and moving in vertical direction with a constant velocity. This motion results in a helix-shaped motion which has the advantage, that the collected radioactivity in the scintillator from daughters, granddaughters and further decay generations of implanted nuclei is transported away from the light-collecting PSPMTs. Rotation frequencies of 20 and 40 rpm which correspond to velocities of 500 and 1000 mm/s on the surface of the scintillator were used for the ^{36}Mg and ^{30}Ne runs, respectively. In addition to this fast rotation long-lived decay products ($T_{1/2} > 200$ ms) can be removed from the active area of the PSPMTs with a vertical motion of 2 mm/s. Because of the fast motion of the scintillator, a direct optical connection of the scintillator and the stationary PSPMTs is not possible: There is an air gap of $\Delta z \approx 3$ mm between the scintillator and the light guides of the PSPMTs. The rotation has to be taken into account for the analysis. A correlation time of 150 ms was sufficient for all the short lived nuclei discussed in this paper. This corresponds to a maximum horizontal shift between the implantation and decay position of 75 and 150 mm for the ^{36}Mg and ^{30}Ne setting, respectively. As this shift is smaller than 3 times the width of a PSPMT, it is not necessary to read out all the PSPMTs. Thus to save read out channels, only the PSPMTs numbered 0, 1, 2, 3 and 4 were read out, as shown in the left part of figure 2. For the data analysis the vertical motion can be neglected as the vertical shift between the implantation and decay position is smaller than 0.3 mm and consequently much smaller than the position resolution of CAITEN (8 mm (FWHM)).

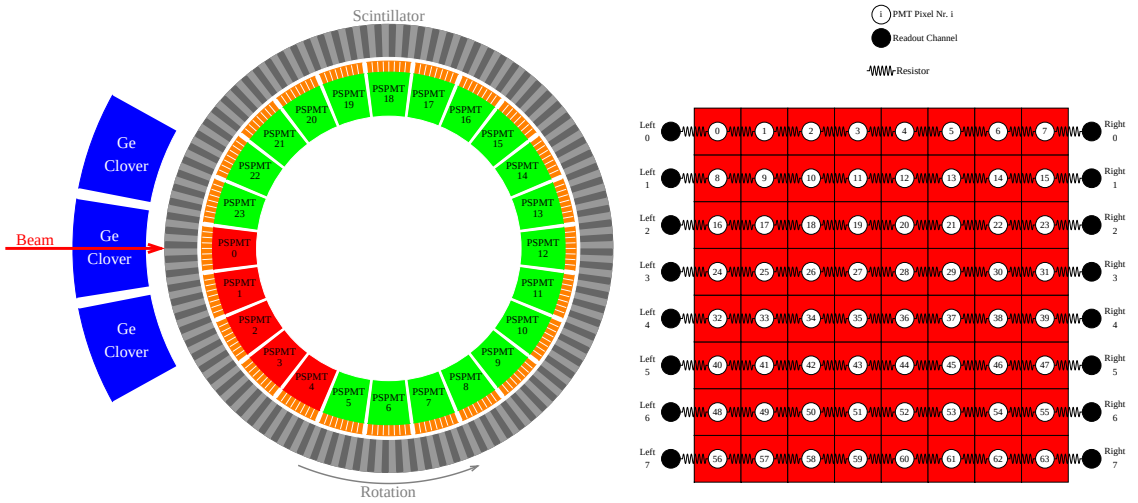

Figure 2: *Left:* Schematic drawing of the components of CAITEN (view from the top). The segmented scintillator is plotted in gray, the PSPMTs which are read out in red, the PSPMTs which are not read out in green, the light guides of the PSPMTs in orange and the HP-germanium clover detectors in blue. *Right:* Readout of a 64-fold segmented PSPMT: 8 horizontal pixels of the PSPMT are connected via a resistor chain (each resistor has $R = 150\,\Omega$) to reduce the number of readout channels from 64 to 16. The splitting of the charge in the left and right channels of the resistor chain is used for the reconstruction of the horizontal position of a decay or implantation event.

2.2.2 Position-sensitive photomultiplier tubes (PSPMTs)

The light detection of the scintillator pixels is done with Hamamatsu H8500 PSPMTs. To collect the emitted scintillation light efficiently, the PSPMTs are coupled to segmented light-guides. The PSPMTs are 64-fold segmented with a pixel size of $5.8 \times 5.8\text{mm}^2$. To reduce the number of readout channels 8 of the anode pixels of a PSPMT were connected via a horizontal resistor chain and read out on both sides (see right part of figure 2). In total there are 16 readout channels for one PSPMT. The PSPMT Nr. 0 at the beam spot position is used for detecting implantations and decays. There is a large difference in energy deposited by an implantation (several GeVs) and a decay (up to several MeVs) event. Therefore the signal of PSPMT Nr. 0 is split in a high gain readout branch for decays and a low gain readout branch for implantations. The PSPMTs Nr. 1-4 are only connected to a high gain readout branch as they detect decays only.

3. Data analysis

The data acquisition systems of BigRIPS used for the particle identification (PID) and the CAITEN detector were used independently in different trigger and deadtime regimes. Implantations in the CAITEN detector and the PID are correlated with time stamps of 10 ns granularity. The two time stamps are compared and if there is a match of a particle identification and an implantation event, these events get correlated. In this way each implantation event can be associated with an identified particle. Due to the air gap of 3 mm between the scintillator and segmented light guides of the PSPMTs not only one pixel of a PSPMT detects the total amount of the emitted light but it is

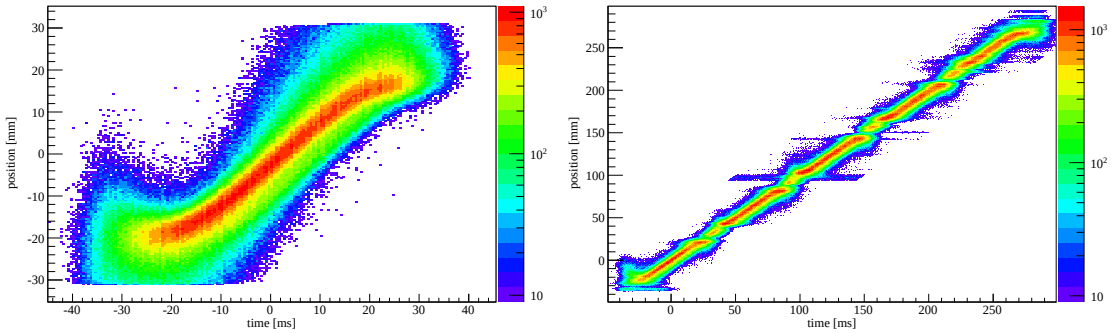

Figure 3: *Left:* Uncalibrated horizontal position of PSPMT Nr. 0 versus the rotation time of the ^{90}Sr calibration source. *Right:* Calibrated horizontal position of all PSPMTs versus the rotation time. The point at time $t = 0$ and position $x = 0$ corresponds to the center of PSPMT Nr. 0. The non-linearity caused by the resistor chain readout of the PSPMTs is corrected by the position calibration. The positions of the five PSPMTs and the gaps in between them are visible.

distributed among a few photomultiplier pixels. In addition, the scintillator pixels and segmented light guides are not aligned because of moving scintillator. Therefore a special method was used to calibrate the position measurement.

3.1 Position calibration

For each horizontal resistor chain of a PSPMT connecting a row of 8 pixels the value $Q_{\text{dep}} = \sqrt{Q_{\text{left}} \cdot Q_{\text{right}}}$ is evaluated. Q_{left} and Q_{right} are the electric charges which were detected by the two sides of a resistor chain. The resistor chain with the highest value for Q_{dep} was defined as the vertical implantation or decay position. A horizontal position calibration was carried out using a ^{90}Sr source that was fixed to the outer surface of the CAITEN scintillator rotating at a frequency of 40 rpm around the PSPMTs. From the timing information of the rotation the exact position x_t of the source was known at all times. The measured (uncalibrated) horizontal position x_{measured} is calculated using

$$x_{\text{measured}} = s \cdot \frac{Q_{\text{right}} - Q_{\text{left}}}{Q_{\text{right}} + Q_{\text{left}}}. \tag{3.1}$$

Q_{right} and Q_{left} are the calibrated charges detected in the left and right channel, respectively. s is a scaling factor to match the size of the PSPMT. With this information and the known position x_t a higher level calibration removing the non-linerities shown in figure 3 (left) was performed. The calibrated horizontal position is shown in figure 3 (right). An average horizontal position resolution of $\Delta x = 8$ mm (FWHM) was determined from this measurement.

3.2 Correlation of implantations and decays

The most important part of the analysis is the correlation of implantations and decays in time and space. The high implantation rate of ≈ 200 Hz together with the limited position resolution of the CAITEN detector leads to a significant amount of wrongly correlated events. To evaluate "real" correlations and random background correlations a background subtraction was performed. A correlation plot and the principle of the background subtraction are illustrated in figure 4 used for the following discussion: The time difference of each implantation with each decay is plotted versus

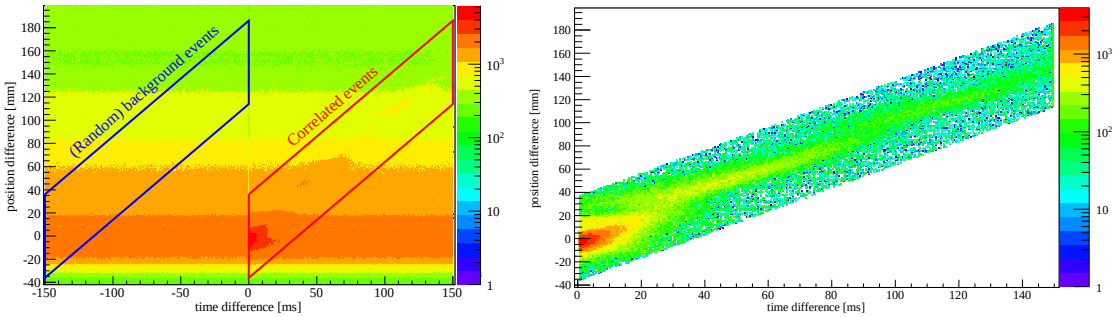

Figure 4: Position-time correlation of implantations and decays of ^{30}Ne. *Left:* Correlation plot of all raw events. The time difference of an implantation and a decay is plotted along the x-axis while the position difference due to the rotation of the scintillator is plotted along the y-axis. The graphical cut on the right-hand side corresponds to correctly correlated events, the one on the left-hand side to (random) background events, only. The area of the two cuts is equal. *Right:* Background subtracted correlation spectrum: The events with a negative correlation time (inside the background cut of the spectrum in the left) are shifted in time by 150 ms and subtracted from the events with the expected correlation time. Bins with zero or a negative number of entries are plotted in white.

the position difference due to the rotation of the scintillator for all registered events. A graphical cut on the right-hand side of the spectrum in the top corresponds to correlated events with a positive correlation time between implantations and decays. This cut takes into account the rotation speed of 1000 mm/s used here. To cover all possible real correlations and avoid systematic uncertainties a spacial correlation window of $\Delta x = \pm 36$ mm was used. To remove random correlations there is a second graphical cut on the left-hand side of the spectrum in the top: As there is a negative correlation time between implantations and decays all events in this cut are random correlations. A subtraction of the events in the graphical cut with negative correlation time from the one with a positive correlation time is performed to quantify the amount of "real" correlations. Due to the data acquisition dead time of $t_{\mathrm{dead}} < 0.5$ ms implantation-decay correlations with a time difference $|t_{\mathrm{diff}}| < t_{\mathrm{dead}}$ are missed. This is taken into account by using time differences $|t_{\mathrm{diff}}| > 1$ ms only for analysis of half-lives.

3.3 Analysis of half-life measurements

Figure 5 shows time projections of the two groups of correlations discussed before cutting on implantations of ^{30}Ne. The black histogram shows the difference of the correlated events after random background subtraction which was used for the half-life analysis. After an implantation there is not only the decay of the implanted very neutron-rich nuclei but there is a decay chain of many generations of nuclei: The mother nucleus ^{A}Z decays to a daughter nuclide ^{A}Z+1, the daughter decays to a granddaughter ^{A}Z+2. This chain continues for many generations until it ends in the valley of stability. In addition to the "normal" β decay it is also possible to have β-delayed neutron emission after the decay of a very neutron-rich nucleus. The probability to have an emission of one or two neutrons after the β decay is denoted with $P(n)$ and $P(2n)$, respectively. Consequently, the mother nucleus ^{A}Z can decay with a probability $P(n)$ to the β-n daughter $^{A-1}$Z+1 and with a probability $P(2n)$ to the β-2n daughter $^{A-2}$Z+1. Only the decays of the mother, daughter

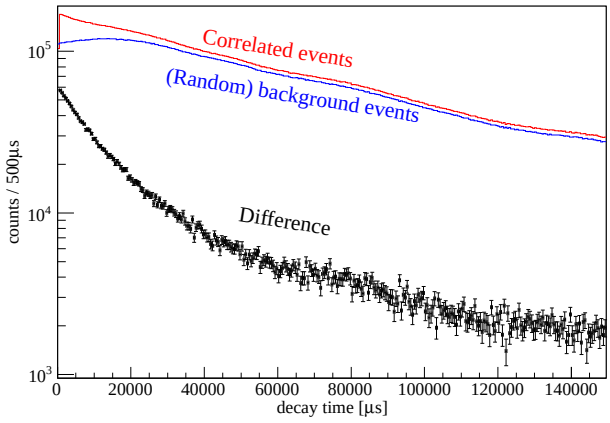

Figure 5: Time correlation of implantations and decays of ^{30}Ne. *Red:* Correlated events. *Blue:* (Random) background events. *Black:* Subtraction of the (random) background events from the correlated events.

and granddaughter generations and the emission of up to two neutrons in a decay chain are taken into account. This is reasonable because the half-lives of the further decay generations are in the order of seconds whereas the half-lives of the investigated mother nuclei are in the order of milliseconds and the probability to have more than two neutrons emitted in one decay chain is very small for all decay chains investigated in this experiment. To extract the decay constants of the nuclei the following mathematical considerations are made: The mother nucleus decays with a decay constant λ which corresponds to a half-life of $t_{1/2} = \ln 2/\lambda$. The probability that the mother nucleus ^{A}Z (denoted with subscript 1) exists at the time t is $P_1(\lambda_1, t) = \exp(-\lambda_1 t)$. Consequently the probability density that a decay of the mother with the decay constant λ_1 takes place in the interval between t and t + dt is given by $f_1(\lambda_1, t) = \lambda_1 P_1(\lambda_1, t) = \lambda_1 \cdot \exp(-\lambda_1 t)$. The probability that the daughter nucleus ^{A}Z+1 (P_{20}), a β-n daughter nucleus $^{A-1}$Z+1 (P_{21}) or a β-2n daughter nucleus $^{A-2}$Z+1 (P_{22}) exists at the time t can be calculated by solving the following differential equation with the initial conditions $P_{2x}(t = 0) = 0$:

$$\frac{\partial P_{2x}(p_{1,x}, \lambda_1, \lambda_{2x}, t)}{\partial t} = p_{1,x}\lambda_1 P_1(\lambda_1, t) - \lambda_{2x} P_{2x}(p_{1,x}, \lambda_1, \lambda_{2x}, t) \tag{3.2}$$

The subscript 2 stands for the daughter generation and the subscript x for the number of neutrons emitted after the mother decay. $p_{1,x}$ denotes the probability to have an emission of x neutrons after the β decay of the mother. So the probability that a daughter nucleus exists at the time t is:

$$P_{2x}(p_{1,x}, \lambda_1, \lambda_{2x}, t) = \frac{p_{1,x}\lambda_1}{\lambda_{2x} - \lambda_1} \left[\exp(-\lambda_1 t) - \exp(-\lambda_{2x} t)\right] \tag{3.3}$$

The probability density that a decay of a daughter nucleus with the decay constant λ_{2x} takes place in the interval between t and t + dt is given by

$$f_{2x}(p_{1,x}, \lambda_1, \lambda_{2x}, t) = \lambda_{2x} P_{2x}(p_{1,x}, \lambda_1, \lambda_{2x}, t) = \frac{p_{1,x}\lambda_1\lambda_{2x}}{\lambda_{2x} - \lambda_1} \left[\exp(-\lambda_1 t) - \exp(-\lambda_{2x} t)\right]. \tag{3.4}$$

The equations for the granddaughter generation can be derived, similarly. The probability density that a decay of a mother, daughter or granddaughter nuclide takes place in the interval between t

and t + dt is given by

$$f_{\text{total}}(t) = f_1(t) + \sum_{x=0}^{2} \left[f_{2x}(t) + f_{3x}(t) \right]. \tag{3.5}$$

For the analysis of the half-life equation 3.5 is fitted to the decay curve with only two fit parameters: The decay constant of the mother nuclide λ_1 and an amplitude C. This amplitude C is only a scaling factor as the probability density $f_{\text{total}}(t)$ is normalized (to the implantation of only one nuclide in the detector). All the other parameters related to less exotic nuclei and typically known with reasonable precision are used as input for the fit.

4. Measured half-lives

The measured half-lives of the implanted nuclei will be presented dependent on the uncertainties of input parameters in addition to the statistical uncertainty of the measurement. To quantify the dependence of the half-life of the implanted nucleus on a parameter x, the parameter Δx is introduced which corresponds to the difference of the "real" value x_{real} and the known literature value x_{lit} divided by the uncertainty of the literature value $\sigma(x_{\text{lit}})$:

$$\Delta x = \frac{x_{\text{real}} - x_{\text{lit}}}{\sigma(x_{\text{lit}})} \tag{4.1}$$

The fit range is chosen to be ≈ 5 times the half-life of the implanted nucleus. Consequently $1-(1/2)^5 \approx 97\%$ of the mother decays appear in this range, which is almost the complete sample. A larger range would lead to an increase of the systematic uncertainties. Figure 6 shows the measured decay curves in comparison with the different contributions (as discussed above) fitted to each distribution. Table 1 gives the results of the fits. The example of ^{30}Ne is used here to explain how to read the table. The measured half-life $t_{1/2}(^{30}\text{Ne})$ in the experiment is 7.40 ms with a statistical uncertainty of 0.04 ms. The literature value for the half-life of the daughter ^{30}Na is 48 ± 2 ms [5]. If the "real" value of the half-life of ^{30}Na is 50 ms (or 46 ms) which corresponds to $t_{1/2}(^{30}\text{Na}) + (-)\sigma(t_{1/2}(^{30}\text{Na}))$ then the measured half-life $t_{1/2}(^{30}\text{Ne})$ increases (decreases) by 0.07 ms. The same method can be applied for the branching ratio $P_{2n}(^{30}\text{Ne})$ and the half-life of the β-n daughter $t_{1/2}(^{29}\text{Na})$. The result for the half-life of ^{30}Ne is

$$\begin{aligned} t_{1/2}(^{30}\text{Ne}) = \big[& 7.40 \pm 0.04(\text{stat.}) \pm 0.07 \left(\text{sys. } \Delta t_{1/2}(^{30}\text{Na})\right) \\ & \pm 0.02 \left(\text{sys. } \Delta P_{2n}(^{30}\text{Ne})\right) \pm 0.01 \left(\text{sys. } \Delta t_{1/2}(^{29}\text{Na})\right) \big] \text{ ms}. \end{aligned} \tag{4.2}$$

Comparing the results of the half-lives measured in this work with literature values there is good agreement within the mutual 1σ uncertainties for all nuclei but ^{35}Mg and ^{36}Mg. The literature half-life $t_{1/2}(^{35}\text{Mg})_{\text{lit}} = 70(40)$ ms [6, 8] has a very large uncertainty which includes the result of this work $t_{1/2}(^{35}\text{Mg})_{\text{this work}} = (11.25 \pm 0.49(\text{stat.}) \pm 0.19(\text{sys.}))$ ms within 1.5σ. $t_{1/2}(^{36}\text{Mg})_{\text{lit}} = 3.9(1.3)$ ms [6, 9] is consistent with the result of this work $t_{1/2}(^{36}\text{Mg})_{\text{this work}} = (7.63 \pm 0.06(\text{stat.}) \, ^{+0.48}_{-0.75}(\text{sys.}))$ ms within 1.8σ. The total uncertainties of the half-lives measured in this work for ^{29}F, ^{30}Ne and ^{35,36}Mg are smaller than the corresponding uncertainties of the literature half-lives. For ^{31,35}Na und ^{37,38}Al the systematic uncertainties dominate the total uncertainties as the uncertainties of the input parameters are large.

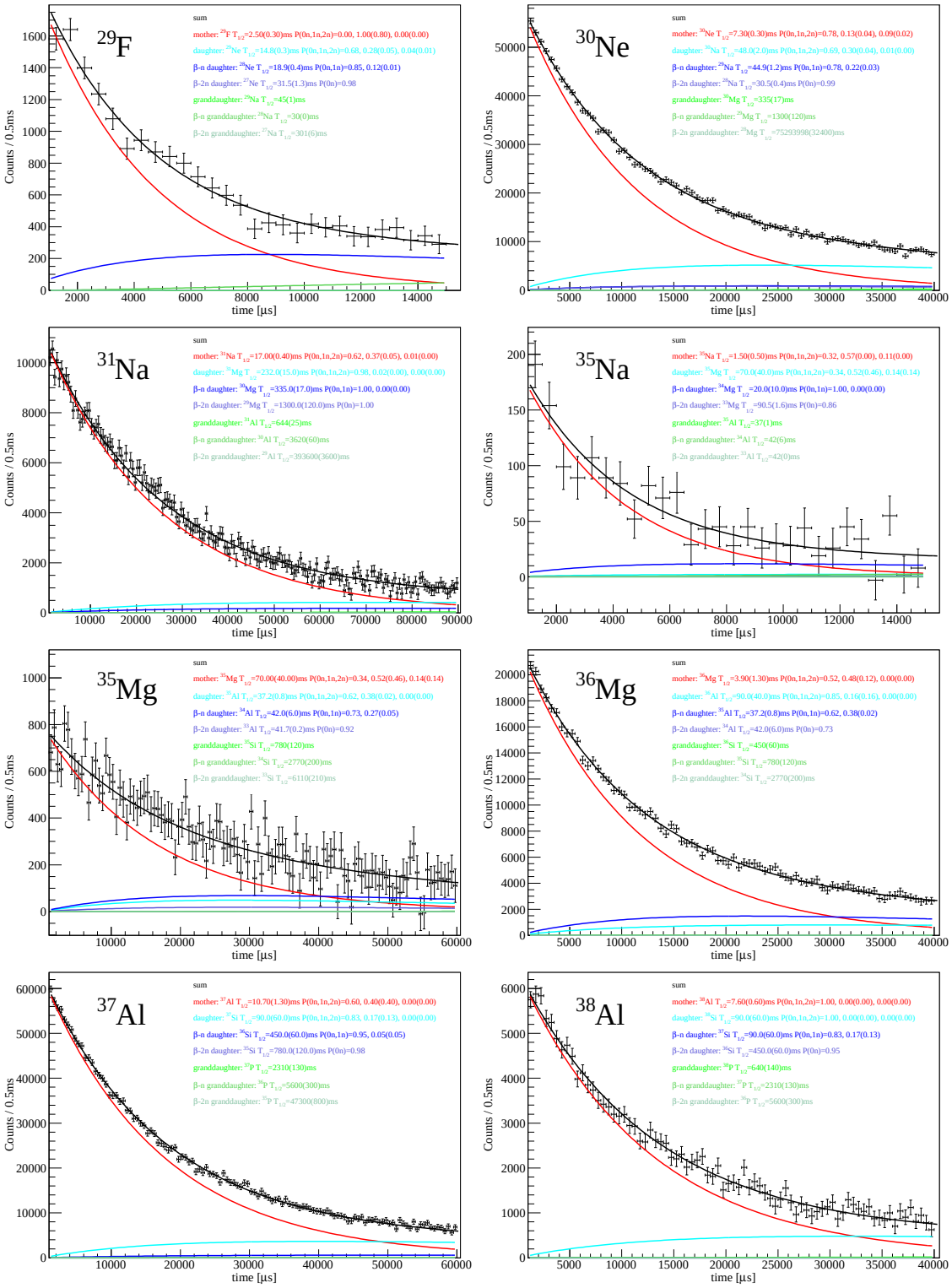

Figure 6: Experimental decay curves and fitted results for ^{29}F, ^{30}Ne, ^{31,35}Na, ^{35,36}Mg and ^{37,38}Al. Aside from the total fit curves the contributions from the mother, daughter and granddaughter decay modes are shown. The literature half-lives of the mother nuclei are the start values for the fits. All the other half-life, $P(n)$ and $P(2n)$ values shown in the figure are input parameters for the fit.

	measured $t_{1/2}$ [ms]	statistical error [ms]	χ^2/ndf	Δt_{20} [ms]	$\Delta P(n)$ [ms]	Δx [ms]	literature $t_{1/2}$ [ms] [6]
^{29}F	2.67	0.10	0.85	0.00	0.16	Δt_{21} 0.02	2.5(3)
^{30}Ne	7.40	0.04	1.16	0.07	0.00	ΔP_{2n} 0.02, Δt_{21} 0.01	7.3(3)
^{31}Na	17.53	0.18	1.08	0.15	0.16	Δt_{21} 0.05	17.0(4)
^{35}Na	2.44	0.31	0.86	0.10	-0.16	Δt_{21} 0.29	1.5(5)
^{35}Mg	11.25	0.49	0.89	0.02	0.17	Δt_{21} 0.21	70(40)
^{36}Mg	7.63	0.06	1.03	$^{+0.27}_{-0.54}$	-0.21		3.9(13)
^{37}Al	11.85	0.06	1.02	$^{+0.93}_{-2.11}$	1.27		10.7(13)
^{38}Al	8.67 *	0.15	0.89	$^{+0.90}_{-2.21}$	0.00		7.6(6)

Table 1: Measured half-lives and uncertainties. All half-lives and uncertainties are given in milliseconds, the χ^2/ndf is a measure for the quality of the fit. t_{20} and t_{21} correspond to the half-life of the daughter and β-n daughter. $P(n)$ and $P(2n)$ are the probabilities to have an emission of one or two neutron after the mother decay. An explanation of how to read the table can be found in the text. (*) Half-life of daughter ^{38}Si not known experimentally, from systematics [7]: $t_{1/2}(^{38}\mathrm{Si}) = 90\,\mathrm{ms}$.

Another method to determine half-lives without input parameters from the decay chain is the measurement of decays with coincident γ-rays which originate from the β decay daughter. But this data is still under analysis and will be published soon [10].

Acknowledgments

This work is funded in part by BMBF (06MT9156), DFG (EXC 153, KR2326/2-1), KAKENHI (19340074) and RIKEN President's Fund (2005).

References

[1] T. Kubo. *Nucl. Inst. Meth. B* **204** (2003) 97.

[2] S. Nishimura. *Prog. Theor. Exp. Phys.* **2012** (2012) 03C006.

[3] Y. Yano. *Nucl. Inst. Meth. B* **261** (2007) 1009.

[4] T. Ohnishi et al. *J. Phys. Soc. Jpn.* **77** (2008) 083201.

[5] M. Langevin et al. *Nuclear Physics A* **414** (1984) 151.

[6] *Evaluated Nuclear Structure Data File, National nuclear data center*, Database version of January 13 (2012).

[7] G. Audi et al. *Nuclear Physics A* **729** (2003) 3.

[8] P. L. Reeder et al. *Proc. Intern. Conf. on Exotic Nuclei and Atomic Masses* (1995) 587.

[9] S. Grévy et al. *Physics Letters B* **594** (2004) 252.

[10] K. Steiger et al. in preparation.